Korean J. Chem. Eng., 38(5), 945-951 (2021)
DOI: 10.1007/s11814-021-0781-9

pISSN: 0256-1115
eISSN: 1975-7220

CO and C_3H_6 oxidation over $La_{0.9}Sr_{0.1}CoO_3$ catalysts: Influence of preparation solvent

Fei Yan*,, Ping Li*,**,†, and Xia Zhang*****

*Hebei Key Lab of Power Plant Flue Gas Multi-Pollutants Control, Department of Environmental Science and Engineering, North China Electric Power University, Baoding, 071003, P. R. China
**MOE Key Laboratory of Resources and Environmental Systems Optimization, North China Electric Power University, Beijing, 102206, P. R. China
***Advanced Research Institute for Multidisciplinary Science, QiLu University of Technology (Shandong Academy of Science), Jinan 250353, Shandong Province, P. R. China
(*Received 2 December 2020 • Revised 9 March 2021 • Accepted 10 March 2021*)

Abstract−High surface area powders, $La_{0.9}Sr_{0.1}CoO_3$ (LSCO), were prepared by a hard template method with a template of SBA-15. In the preparation process, the solvent was ethanol, the mixture of ethanol and water, and water, respectively. Characterizations were performed to understand the properties of the catalysts. When the solvent is a mixture of ethanol and water, the prepared LSCO has the most easily extracted surface adsorbed oxygen in the H_2 atmosphere, exhibiting the best light-off performances for CO oxidation. However, the LSCO prepared in ethanol solvent has the best lattice oxygen mobility, resulting in the best light-off performance for C_3H_6 oxidation. Moreover, the LSCO prepared in ethanol also shows the best catalytic activity for both CO and C_3H_6 oxidation under the conditions of simulated diesel exhaust. Furthermore, Pd was impregnated on the LSCO, which was prepared by a sol-gel method and a hard template method, separately; the later one shows higher CO and C_3H_6 catalytic oxidation activity.

Keywords: $La_{0.9}Sr_{0.1}CoO_3$, Solvent, CO Oxidation, C_3H_6 Oxidation, Simulated Diesel

INTRODUCTION

With the advantage of higher fuel efficiency, diesel engines are widely used and CO, hydrocarbon (HC) and NOx are considered as their exhaust gases [1]. In the diesel engine system, some aftertreatment devices are installed [2]. Among them, diesel oxidation catalyst (DOC), which can make CO, unburned HC and NO oxidized to CO_2, H_2O and NO_2, is considered as the important part [3]. Generally, supported noble metals are applied to a commercial DOC because of their good oxidation activity. However, some drawbacks still exist such as expense and ease of agglomeration [4,5] and perovskite oxide is considered as a promising alternative [6,7].

The general formula for perovskite oxides is ABO_3 and the oxidation activity of the perovskite is mainly controlled by B site cations [8,9]. Furthermore, when lanthanum as A site cation and Co, Mn, Fe, Cr or Ni as B site cations, the perovskite oxides achieved a high catalytic activity [10,11]. Meanwhile, among them, $LaCoO_{3-\delta}$ has been reported as a promising perovskite oxide for the oxidation reaction [12,13]. To further increase the catalytic activity of $LaCoO_{3-\delta}$, Sr is used to partially substitute La. It has been well established that the Sr doping in $LaCoO_{3-\delta}$ can generate oxygen vacancies, favoring the oxidation activity [14]. Sr-doped $LaCoO_{3-\delta}$ perovskites have been widely used for many applications [15-17]. Kim et al. [2] tested the NO oxidation activity of $La_{0.9}Sr_{0.1}CoO_3$ under realistic automotive conditions, and the results showed that $La_{0.9}Sr_{0.1}CoO_3$ displayed a comparable activity to Pt-based catalysts. Onrubia et al. [14] prepared a series of $La_{1-x}Sr_xCoO_3$ perovskites (x=0.1, 0.2, 0.3, 0.4 and 0.5) with citric acid sol-gel method and used NO-to-NO_2 oxidation reaction as the target reaction. The results showed that $La_{0.7}Sr_{0.3}CoO_3$ achieved the highest catalytic activity, which showed the maximum NO conversion of 83% at 300 °C. They attributed the high oxidation activity of $La_{0.7}Sr_{0.3}CoO_3$ to the high oxygen mobility. As discussed above, Sr-doped $LaCoO_{3-\delta}$ displayed a good catalytic activity toward NO to NO_2 oxidation reaction. However, for CO and HC oxidation reaction, it showed high conversion temperature, which restricts its application in DOC [8, 15,18,19].

When using perovskite oxide as the DOC, the structural properties, such as particle size and surface area, influence catalytic oxidation activity [12]. Meanwhile, Xiao et al. [19] also pointed out that increasing the surface area of perovskite oxide is an effective way to improve the low-temperature catalytic oxidation activity. Therefore, high surface area of Sr-doped $LaCoO_{3-\delta}$ catalysts needs to be synthesized to enhance the catalytic activity toward CO and HC oxidation. To obtain catalysts with high surface area, silica-based mesoporous materials, such as SBA-15 and KIT-6, can be applied as the template due to their well-ordered pore structure and high surface area [20,21]. In our previous work, we prepared $La_{0.9}Sr_{0.1}CoO_3$ (LSCO) perovskite with SBA-15 as the template and the solvent was the mixture of ethanol and water in the preparation procedure [22]. This catalyst exhibited higher CO and C_3H_6 catalytic oxidation activity than the LSCO prepared with sol-gel method. In this work, LSCO oxides were prepared in different solvents by a hard template method, and the influence of solvent on the CO and C_3H_6 catalytic oxidation activity was investigated. In addition, we also investigated both CO and C_3H_6 catalytic oxidation activity under

†To whom correspondence should be addressed.
E-mail: liping@ncepu.edu.cn

simulated diesel exhaust conditions with different LSCO catalysts.

EXPERIMENTAL

1. Preparations of Catalysts

The template, SBA-15, was prepared following a procedure which has been shown in the literature [23]. LSCO powders were synthesized with SBA-15 as the template. For a typical synthesis, $La(NO_3)_3 \cdot 6H_2O$, $Sr(NO_3)_2$, $Co(NO_3)_2 \cdot 6H_2O$, and citric acid were dissolved in ethanol, a mixture of ethanol and deionized water (v/v=1/1), and deionized water, respectively. The preparation procedure of LSCO has been shown in our previous work. The samples prepared in ethanol, a mixture of ethanol and deionized water (v/v=1/1), and deionized water were labeled as LSCO (E), LSCO (E/W) and LSCO (W), respectively. In addition, LSCO powders were also synthesized by the sol-gel method and denoted as LSCO (S). The synthesis processes have been also described in our previous work. All the catalysts were calcined at 700 °C for 6 h to form the perovskite structure. Furthermore, 1.4 wt% Pd was impregnated on LSCO (E) and LSCO (S) using $Pd(NO_3)_2$ (Alfa Aesar) precursor aqueous solution. The as-prepared samples were calcined at 500 °C for 4 h [24] and labeled as Pd/LSCO (E) and Pd/LSCO (S), respectively.

2. Catalytic Reaction Tests

The light-off performance was tested in a fixed-bed quartz tube reactor and the catalysts were put into the tube with a weight of 50 mg [25]. For CO oxidation reaction, the inlet gas was balanced with N_2, and the concentration of CO and O_2 was 0.4% and 10%, respectively. The conversion of CO followed an equation of

$$X_{CO}=(C_{CO,in}-C_{CO,out})/(C_{CO,in})\times 100\% \quad (1)$$

where $C_{CO,in}$ and $C_{CO,out}$ represent the inlet CO concentration and outlet CO concentration.

For C_3H_6 oxidation reaction, the inlet gas was balanced with N_2, and the concentration of C_3H_6 and O_2 was 0.1% and 10%, respectively. The corresponding conversion of C_3H_6 followed an equation of

$$X_{C_3H_6}=(C_{C_3H_6,in}-C_{C_3H_6,out})/(C_{C_3H_6,in})\times 100\% \quad (2)$$

where $C_{C_3H_6,in}$ and $C_{C_3H_6,out}$ represent the inlet C_3H_6 concentration and outlet C_3H_6 concentration.

For the simultaneous oxidation tests, the simulated diesel emissions were also balanced with N_2 and the concentration of CO, C_3H_6, NO, O_2, and H_2O was 0.4%, 0.1%, 0.05%, 10%, and 5%, respectively. The WHSV for all these three reactions was 240,000 mL $g^{-1} \cdot h^{-1}$ and a gas analyzer was applied to detect the outlet gases. The conversions of CO, C_3H_6 have been described above and the conversion of NO to NO_2 is defined by the following equation;

$$X_{NO\text{-}NO_2}=(C_{NO_2,out}-C_{NO_2,in})/(C_{NO,in})\times 100\% \quad (3)$$

where $C_{NO,in}$, $C_{NO_2,in}$, and $C_{NO_2,out}$ represent the inlet NO, inlet NO_2 and outlet NO_2 concentrations, respectively.

3. Characterization

A Rigaku (Smartlab) instrument was used to record the X-ray diffraction (XRD) patterns of the catalysts. The samples were subjected to Cu-Kα radiation with a voltage of 40 kV and a current of 44 mA in a continuous scan mode from 15° to 90° with a step size of 0.02°. Textural properties of the samples were detected at −196°C by N_2-physisorption instrument (ASAP2020). The samples were degassed under vacuum condition before the measurement following our previous procedure. The morphology of various LSCO powders was studied with a Hitachi S-4800 scanning electron microscope (SEM). A JEM 2100F electron microscope (JEOL, Japan) was used to record the transmission electron microscopy (TEM) images. H_2-temperature-programmed reduction (H_2-TPR) was used to measure the reducibility of catalysts following the same operation procedure as described in our previous work [23,25]. TGA measurement was performed on TA Instruments (Q500) to test the oxygen loss rate in H_2 atmosphere. Before the measurement, the sample was first pretreated in N_2 atmosphere at 300 °C for 1 h and then cooled to 50 °C. Then the oxygen loss rate was measured in 10%H_2/90%N_2 atmosphere from 50 °C to 500 °C following the procedure shown in Fig. S1 [25]. Furthermore, to analyze the deep-available oxygen, the catalysts were heated to 850 °C in a flow of N_2 with a ramp rate of 10 °C min^{-1}, and the total weight loss was recorded by TGA.

RESULTS AND DISCUSSION

1. Structural Properties

Fig. 1 displays the XRD patterns of various LSCO catalysts. The XRD patterns of these three samples match well with the standard XRD patterns of $La_{0.9}Sr_{0.1}CoO_3$ (JCPDS # 28-1229). As to LSCO (E), it shows the lowest peak intensities, indicating that LSCO (E) shows the lowest degree of crystallinity. Therefore, in the synthesis process, the addition of water increases the degree of crystallinity of LSCO, suggesting that water is important for obtaining a perovskite phase. This may be because the nitrate can be completely ionized in adequate water [26]. Furthermore, some Co_3O_4 peaks are observed in all the LSCO catalysts, suggesting that a relatively low concentration of Co_3O_4 exists in the catalysts.

The N_2 adsorption-desorption isotherms and the corresponding Brunauer-Emmett-Teller (BET) surface area of the various catalysts are shown in Fig. 2. The BET surface areas of LSCO (E),

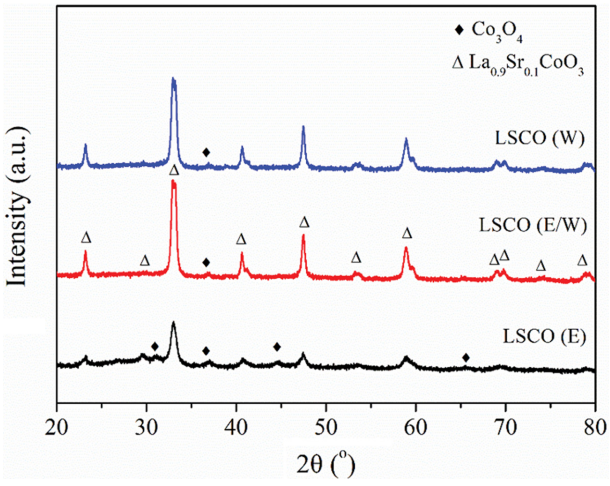

Fig. 1. XRD patterns of LSCO (E), LSCO (E/W) and LSCO (W).

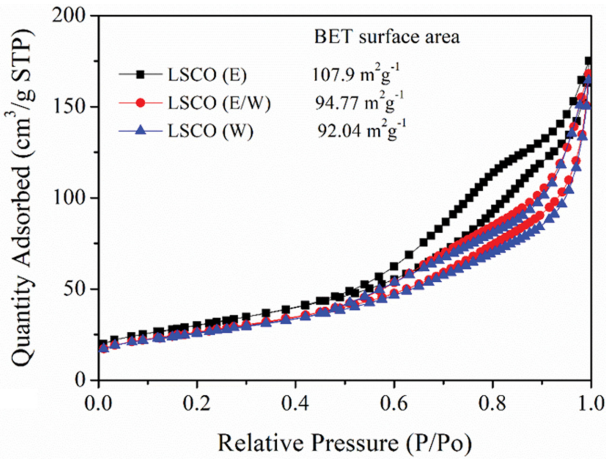

Fig. 2. N_2 adsorption-desorption isotherms of different catalysts.

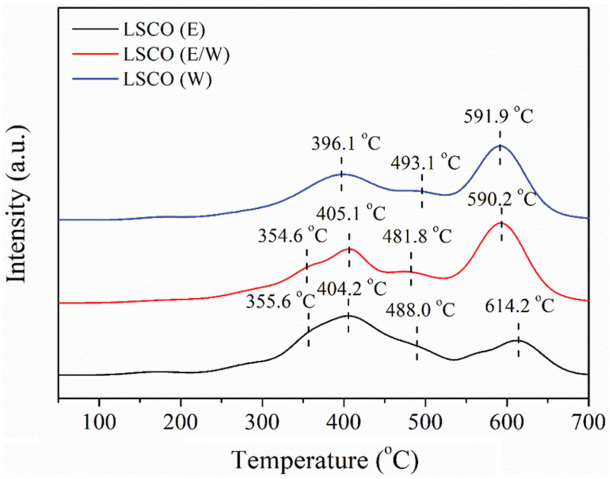

Fig. 4. H_2-TPR profiles of different catalysts.

LSCO (E/W) and LSCO (W) are 107.9, 94.77 and 92.04 m^2 g^{-1}, respectively, showing that the addition of water in the synthesis process decreases the surface area. Fig. S2 and Fig. 3 show the SEM and TEM images of these three catalysts. The particle sizes of these three catalysts are in the range of 30-50 nm. The morphologies of these three catalysts are different from that of the SBA-15 template [27], indicating that the porous structure of the catalysts stem solely from the stacking of nanoparticles [23].

2. Reducibility

2-1. H_2-TPR

Fig. 4 shows the H_2-TPR results of the LSCO catalysts, which reflects the reducibility of the various catalysts. There are three main peaks that correspond to the reduction of Co^{3+} to Co^{2+}, reduction of Co^{2+} to Co^0 in Co_3O_4 and further reduction of Co^{2+} to Co^0 in LSCO structure, respectively [14,19]. For the first peak, the reduction temperature of LSCO (E) is close to that of LSCO (E/W) and LSCO (W) shows the highest reduction temperature, suggesting that the reduction of Co^{3+} to Co^{2+} is easier to happen in LSCO (E) and LSCO (E/W) than in LSCO (W). The reduction temperature of the second peak for these three catalysts is 488.0, 481.8 and 493.1 °C, which are much similar, because the reduction of Co^{2+} in Co_3O_4 happens at the temperature range of the second peak [25] and the presence of Co_3O_4 has been observed in XRD patterns. Furthermore, for the third peak, the reduction temperatures of LSCO (E), LSCO (E/W) and LSCO (W) are 614.2, 590.2 and 591.9 °C, respectively, suggesting that the addition of water in the synthesis process can decrease the reduction temperature of Co^{2+} to Co^0. As a result, LSCO (E) and LSCO (E/W) process the highest reducibility for $Co^{3+}\rightarrow Co^{2+}$. In addition, for $Co^{2+}\rightarrow Co^0$, LSCO (E/W) exhibits the highest reducibility.

2-2. Oxygen Loss Rate

It has been established that the catalytic oxidation activity of the catalysts is much correlated to the mobility of the oxygen, and the oxygen migration capacity of the catalyst can be reflected by the oxygen loss rate of the catalyst under a hydrogen atmosphere [28,29]. In this work, TGA techniques were used to measure the oxygen loss rate. The oxygen release loss of all the catalysts in H_2 environment from 50 °C to 500 °C is shown in Fig. 5. The oxygen loss rate increases with the increasing temperature for these three catalysts. When T<200 °C, the order of oxygen loss rate is LSCO (E/W)> LSCO (E)>LSCO (W). The released oxygen belongs to the surface oxygen and the higher oxygen loss rate means higher oxygen mobility from the surface of LSCO [30]. When 200 °C≤T≤450 °C, LSCO (E) shows the highest oxygen loss rate and LSCO (W) shows the lowest oxygen loss rate. Combined with H_2-TPR results, the oxygen released in this region is probably due to the reduction of

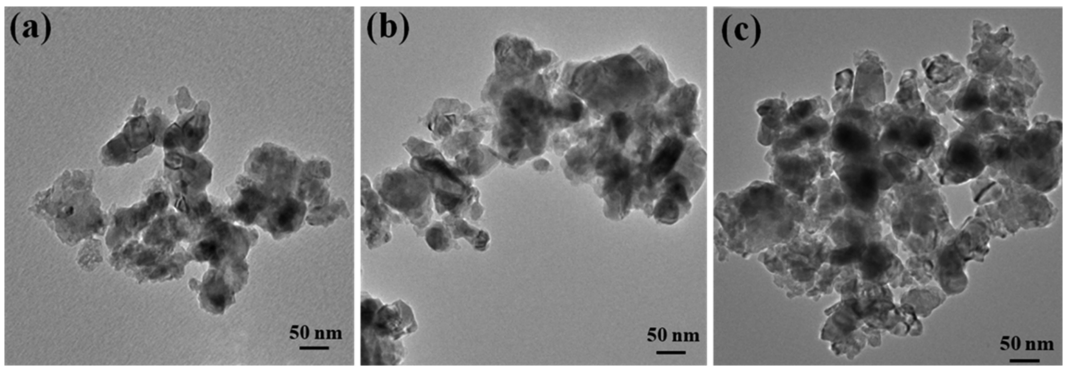

Fig. 3. TEM images of (a) LSCO (E), (b) LSCO (E/W) and (c) LSCO (W).

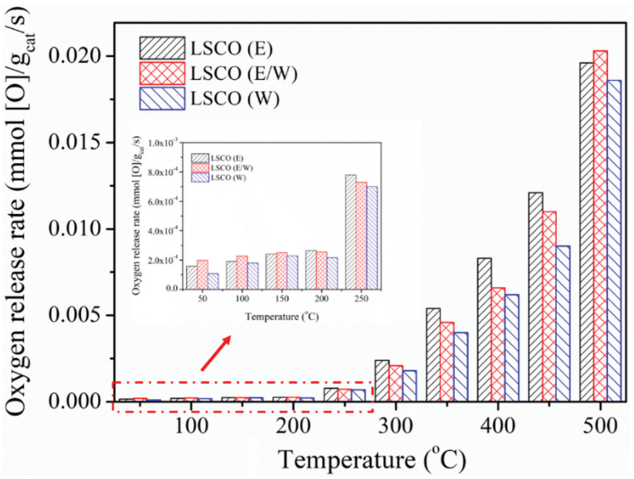

Fig. 5. Oxygen loss rate of different catalysts under versus temperature.

Co^{3+} cations, implying that the lattice oxygen surrounding Co^{3+} cations in LSCO (E) has the highest mobility. When T>450 °C, LSCO (E/W) displays the highest oxygen loss rate and the oxygen released above 450 °C is mainly the lattice oxygen surrounding Co^{2+} cations in LSCO. Therefore, at low temperature region (T< 200 °C) and high temperature region (T>450 °C), oxygen in LSCO (E/W) has the highest mobility, while at intermediate temperature region (200 °C≤T≤450 °C), oxygen in LSCO (E) has the highest mobility in H_2 environment. It has been reported that more oxygen vacancies would facilitate the mobility of lattice oxygen and then further improve the catalytic activity of oxidation reactions [23]. To investigate the mobility of lattice oxygen, the operation of TGA in N_2 flow was used by heating the material from room temperature to 850 °C. The measured weight loss curves are shown in Fig. S3. Generally, the weight loss below 700 °C is considered due to desorption of surface-adsorbed OH and nonstoichiometric oxygen. The weight loss above 700 °C is attributed to the release of lattice oxygen in LSCO, indirectly reflecting the oxygen vacancies [31]. LSCO (E) shows the most weight loss and LSCO (W) exhibits the least weight loss, indicating that LSCO (E) shows more oxygen vacancies. Furthermore, from the corresponding derivative thermogravimetry (DTG) curves shown in Fig. S3, LSCO (E) shows the lowest peak, indicating that LSCO (E) could facilitate the mobility of lattice oxygen.

3. Catalytic Activity for CO and C_3H_6 Oxidation

3-1. LSCO Catalyst

CO and C_3H_6 oxidation reactions over the LSCO (E), LSCO (E/W) and LSCO (W) catalysts were performed, and the light-off curves are shown in Fig. 6. The light-off temperature is defined as the temperature at 50% conversion (T_{50}) and its values of 148, 146 and 153 °C are achieved on LSCO (E), LSCO (E/W) and LSCO (W) for the CO oxidation reaction, respectively. LSCO (E/W) shows the lowest T_{50} indicating a highest catalytic activity for CO oxidation. As to C_3H_6 oxidation, the corresponding T_{50} values are 239, 258 and 276 °C for LSCO (E), LSCO (E/W) and LSCO (W), respectively. LSCO (E) shows the lowest light-off temperature, exhibiting the highest C_3H_6 catalytic oxidation activity.

It has been demonstrated that for CO oxidation reaction, the surface oxygen adsorbed on LSCO catalysts reacts with the adsorbed CO to generate CO_2, but in the C_3H_6 oxidation reaction, the involved oxygen is the lattice oxygen, mainly derived from $Co^{3+}\rightarrow Co^{2+}$ [22]. In this work, the highest mobility of the surface adsorbed oxygen was found in LSCO (E/W) (Fig. 5), exhibiting the lowest T_{50} for CO oxidation reaction. Furthermore, combined with the results shown in Fig. 4 and Fig. 5, the highest mobility of the lattice oxygen surrounding Co^{3+} cations was observed in LSCO (E), confirming that LSCO (E) shows the highest catalytic activity towards C_3H_6 oxidation.

For further examining the hydrothermal stability of various LSCO samples, all the catalysts were hydrothermally treated in flowing of 10% H_2O/Air at 750 °C for 120 min and the results are shown in Fig. S4. The T_{50} values of 158, 155 and 168 °C were achieved on aged-LSCO (E), aged-LSCO (E/W) and aged-LSCO (W) for the CO oxidation reaction, respectively. As to C_3H_6 oxidation, the corresponding T_{50} values were 242, 268 and 294 °C for aged-LSCO (E), aged-LSCO (E/W) and aged-LSCO (W), respectively. The trend of catalyst activity after hydrothermal treatment is consistent with

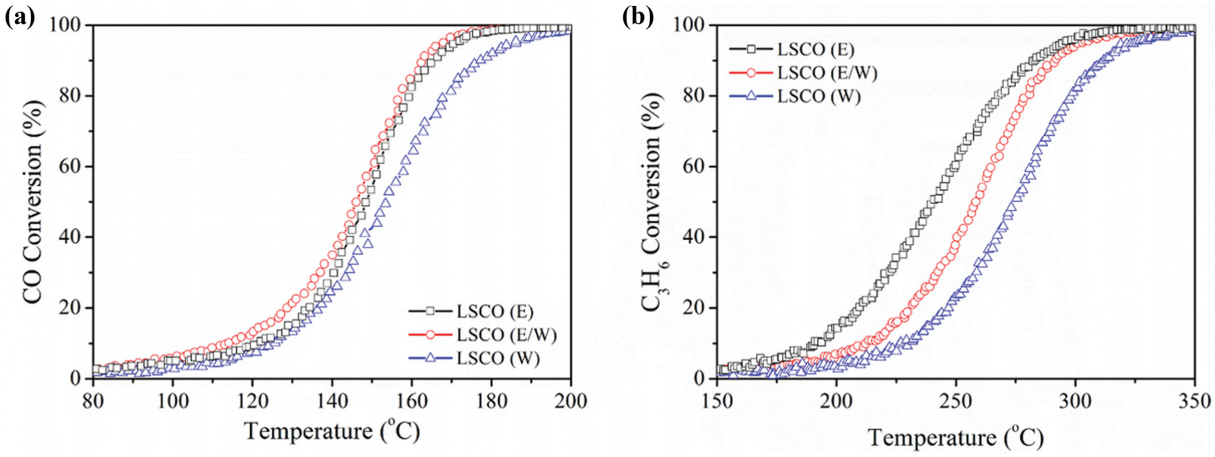

Fig. 6. Light-off curves of (a) CO and (b) C_3H_6 oxidation over different catalysts. Reaction conditions: (a) 0.4% CO, 10% O_2 balanced with N_2 and (b) 0.1% C_3H_6, 10% O_2 balanced with N_2.

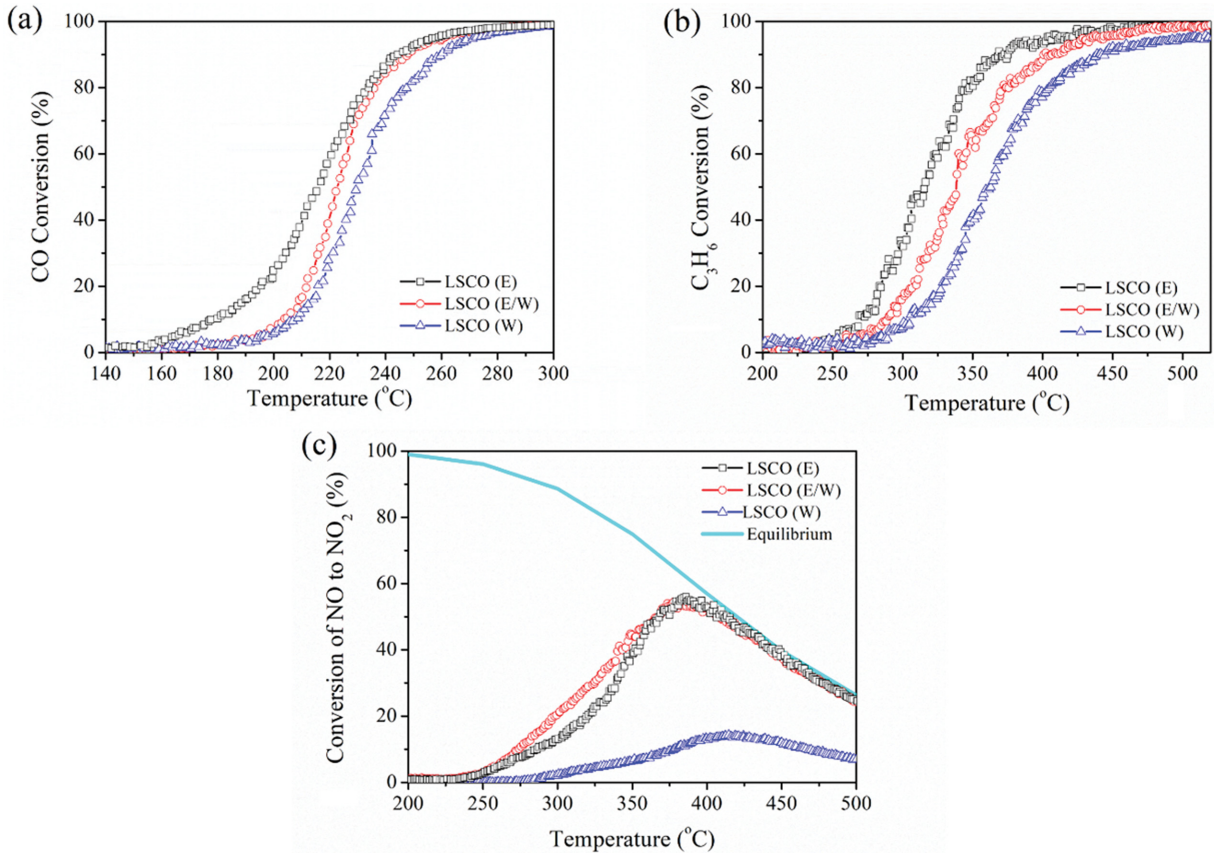

Fig. 7. Catalytic oxidation activities of CO, C_3H_6 and NO on different catalysts in the simulated diesel exhaust (a) Light-off curves of CO; (b) Light-off curves of C_3H_6; (c) Conversions of NO to NO_2.

that before treatment.

Furthermore, to evaluate the catalytic activity for the simultaneous oxidation of CO, C_3H_6, and NO over various LSCO catalysts, the various catalysts were tested in simulated diesel exhaust conditions. Fig. 7 shows the light-off curves for the simultaneous CO, C_3H_6, and NO oxidation on the LSCO catalysts. T_{50} of LSCO (E), LSCO (E/W) and LSCO (W) are 217, 223, and 230 °C, respectively for CO oxidation reaction. In addition, the T_{50} of LSCO (E), LSCO (E/W) and LSCO (W) for C_3H_6 oxidation are 315, 338, and 363 °C, respectively. For the oxidation of NO to NO_2, the maximum conversions are 57.0, 56.6 and 14.3% over LSCO (E), LSCO (E/W) and LSCO (W), respectively, and the corresponding temperatures are 387, 383 and 414 °C, respectively. Among them, LSCO (E) shows the best catalytic oxidation ability for CO, C_3H_6, and NO oxidation. Furthermore, compared to the results shown Fig. 6, the T_{50} values of various LSCO catalysts are increased for CO and C_3H_6 oxidation in the simulated diesel exhaust, indicating that the co-existence of CO, C_3H_6, NO and H_2O will inhibit the catalytic oxidation reaction. LSCO (W) exhibits the lowest catalytic activity for CO and C_3H_6 oxidation; in order to explore the role of H_2O in the feed stream, the CO and C_3H_6 oxidation performance for LSCO (W) catalyst was investigated in $CO+O_2+H_2O$ and $C_3H_6+O_2+H_2O$ conditions and the results are shown in Fig. S5. When the reaction was carried out in $CO+O_2+H_2O$, the T_{50} of CO oxidation for LSCO (W) increased from 153 °C to 201 °C, indicating that the existence of H_2O will inhibit the CO oxidation reaction. Furthermore, the presence of H_2O also affected the T_{50} of C_3H_6 oxidation in $C_3H_6+O_2+H_2O$, which then increased from 276 °C to 335 °C.

3-2. Pd/LSCO Catalyst

As discussed above, LSCO (E) shows the best catalytic activity for CO, C_3H_6, and NO oxidation in the simulated diesel exhaust. In addition, it has been demonstrated that loading of PGM metals, such as Pd, can improve the catalytic activity toward oxidation reaction due to the hydrogen spill-over mechanism [28,32]. Because LSCO (E) shows the best catalytic oxidation activity, Pd/LSCO (E) catalyst was synthesized. Furthermore, Pd/LSCO (S) catalyst was also prepared to compare the effect of the synthesis method of LSCO. The TEM images of Pd/LSCO (E) and Pd/LSCO (S) are shown in Fig. S6, and Pd particles in each catalyst are similar in size and evenly distributed. In addition, the oxygen loss rates of Pd/LSCO (E) and Pd/LSCO (S) are shown in Fig. S7. Pd/LSCO (E) exhibits higher oxygen loss rate than Pd/LSCO (S). Furthermore, the oxygen loss rate of Pd/LSCO (E) is higher than LSCO (E), confirming that Pd loading facilitates the oxygen release, which is probably because of the H_2 spillover mechanism.

Fig. 8 reflects the performance curves of Pd/LSCO (E) and Pd/LSCO (S) catalysts for the catalytic oxidation of CO and C_3H_6. For the CO oxidation reaction, Pd/LSCO (E) exhibits similar catalytic oxidation activity as Pd/LSCO (S), and their T_{50} values are both 147 °C. However, for the oxidation reaction of C_3H_6, Pd/LSCO (E)

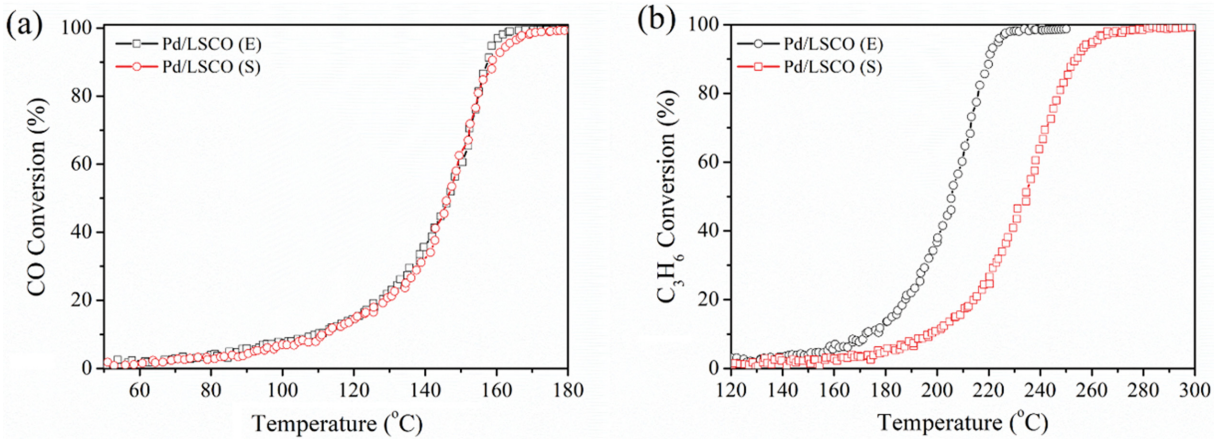

Fig. 8. Light-off curves of (a) CO and (b) C_3H_6 oxidation on Pd/LSCO (E) and Pd/LSCO (S). Reaction conditions: (a) 0.4% CO, 10% O_2 balanced with N_2 and (b) 0.1% C_3H_6, 10% O_2 balanced with N_2.

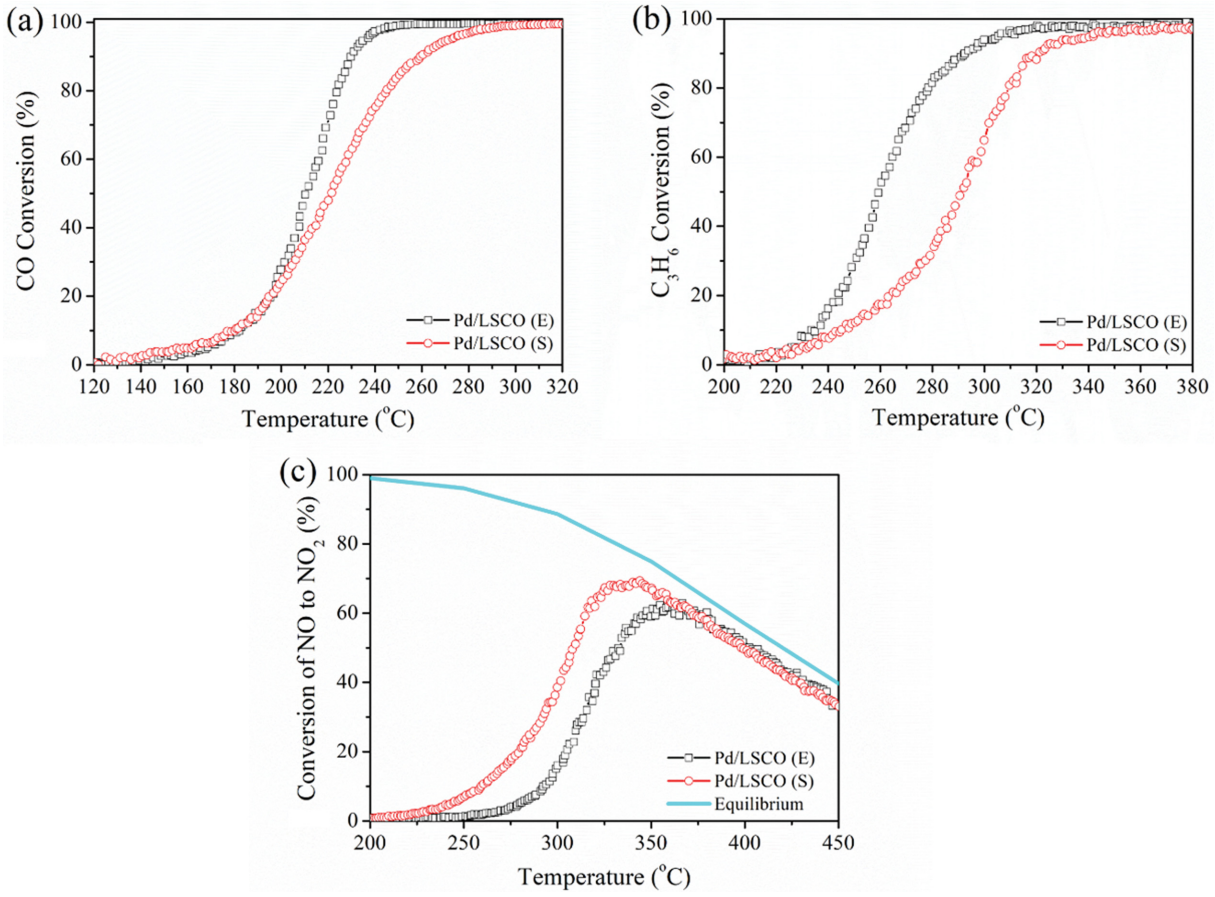

Fig. 9. Catalytic oxidation activity of CO, C_3H_6 and NO on Pd/LSCO (E) and Pd/LSCO (S) catalysts in the simulated diesel exhaust. (a) Light-off curves of CO; (b) light-off curves of C_3H_6; (c) conversions of NO to NO_2.

shows a good catalytic activity, its T_{50} is 205 °C, which is about 20 °C lower than the T_{50} of Pd/LSCO (S). Furthermore, compared to the light-off performance on LSCO (E), Pd/LSCO (E) shows almost the same T_{50} value for CO oxidation reaction, but lower T_{50} value for C_3H_6 oxidation, indicating that Pd loading can facilitate the mobility of the lattice oxygen, which mainly surrounds Co^{3+} cations in LSCO.

Similarly, Fig. 9 shows the light-off curves for the simultaneous CO, C_3H_6, and NO oxidation on the Pd/LSCO catalysts. As to CO oxidation reaction, T_{50} of Pd/LSCO (E) is 210 °C, which is 12 °C lower than that of Pd/LSCO (S). In addition, for C_3H_6 oxidation, the T_{50} of Pd/LSCO (E) and Pd/LSCO (S) are 259 and 292 °C,

respectively. The maximum conversion of NO oxidation corresponding to Pd/LSCO (E) and Pd/LSCO (S) are 61.5% and 68.0%, respectively, while the corresponding temperatures to the maximum conversion are 358 and 336 °C, respectively. Therefore, for both CO and C_3H_8 oxidation, Pd/LSCO (E) shows higher catalytic activity but for the NO oxidation, Pd/LSCO (S) displays the higher catalytic activity. The reason for this phenomenon needs to be further investigated.

CONCLUSIONS

$La_{0.9}Sr_{0.1}CoO_3$ (LSCO) powders were prepared by a hard template method with a template of SBA-15. In the preparation process, the solvents were ethanol, a mixture of ethanol and water, and water, respectively. All the catalysts show a perovskite structure and a little content of Co_3O_4. From various characterization results, the oxygen adsorbed on the surface of LSCO (E/W) was the easiest to extract in the H_2 atmosphere. However, LSCO (E) showed the best lattice oxygen mobility, which in turn led to the best C_3H_6 oxidation performance of LSCO (E). For the CO oxidation reaction, the T_{50} of CO catalytic oxidation under the action of LSCO (E), LSCO (E/W) and LSCO (W) catalysts were 148, 146 and 153 °C, respectively. For C_3H_6 oxidation, the T_{50} values corresponding to LSCO (E), LSCO (E/W) and LSCO (W) were 239, 258 and 276 °C, respectively. Furthermore, LSCO (E) showed the best catalytic activity for the simultaneous oxidation of CO and C_3H_6 under the conditions of simulated diesel exhaust. In addition, Pd/LSCO (E) displayed better CO and C_3H_6 catalytic oxidation activity than Pd/LSCO (S).

ACKNOWLEDGEMENT

This study was supported by the Fundamental Research Funds for the Central Universities (No. 2020MS124 and 2020MS126) and Natural Science Foundation of Hebei Province (No. B2020502002 and B2020502003)

SUPPORTING INFORMATION

Additional information as noted in the text. This information is available via the Internet at http://www.springer.com/chemistry/journal/11814.

REFERENCES

1. J. Xu, G. Lu, Y. Guo, Y. Guo and X.-Q. Gong, *Appl. Catal. A-Gen.*, **535**, 1 (2017).
2. C. H. Kim, G.Qi, K. Dahlberg and W. Li, *Science*, **327**, 1624 (2010).
3. A. Russell and W. S. Epling, *Catal. Rev.*, **53**, 337 (2011).
4. W. Tang, W. Xiao, S. Wang, Z. Ren, J. Ding and P.-X. Gao, *Appl. Catal. B-Environ.*, **226**, 585 (2018).
5. X. Auvray and L. Olsson, *Appl. Catal. B-Environ.*, **168-169**, 342 (2015).
6. D. Pinto and A. Glisenti, *Catal. Sci. Technol.*, **9**, 2749 (2019).
7. A. Glisenti and A. Vittadini, *Catalysts*, **9**, 312 (2019).
8. H. Ziaei-Azad, A. Khodadadi, P. Esmaeilnejad-Ahranjani and Y. Mortazavi, *Appl. Catal. B-Environ.*, **102**, 62 (2011).
9. P. Li, Q. Yang, H. Zhang, M. Yao, F. Yan and D. Fu, *Int. J. Hydrogen Energy*, **45**, 11802 (2020).
10. S. Cimino, L. Lisi, S. De Rossi, M. Faticanti and P. Porta, *Appl. Catal. B-Environ.*, **43**, 397 (2003).
11. B. Kucharczyk and W. Tylus, *Catal. Today*, **90**, 121 (2004).
12. J. Chen, M. Shen, X. Wang, J. Wang, Y. Su and Z. Zhao, *Catal. Commun.*, **37**, 105 (2013).
13. J. Chen, M. Shen, X. Wang, G. Qi, J. Wang and W. Li, *Appl. Catal. B-Environ.*, **134-135**, 251 (2013).
14. J. A. Onrubia, B. Pereda-Ayo, U. De-La-Torre and J. R. González-Velasco, *Appl. Catal. B-Environ.*, **213**, 198 (2017).
15. S. Ponce, M. A. Peña and J. L. G. Fierro, *Appl. Catal. B-Environ.*, **24**, 193 (2000).
16. F. Teng, W. Han, S. Liang, B. Gaugeu, R. Zong and Y. Zhu, *J. Catal.*, **250**, 1 (2007).
17. C. Zhang, W. Hua, C. Wang, Y. Guo, Y. Guo, G. Lu, A. Baylet and A. Giroir-Fendler, *Appl. Catal. B-Environ.*, **134-135**, 310 (2013).
18. N. Mota, M. C. Alvarez-Galván, R. M. Navarro, S. M. Al-Zahrani, A. Goguet, H. Daly, W. Zhang, A. Trunschke, R. Schlögl and J. L. G. Fierro, *Appl. Catal. B-Environ.*, **113-114**, 271 (2012).
19. P. Xiao, J. Zhu, H. Li, W. Jiang, T. Wang, Y. Zhu, Y. Zhao and J. Li, *Chemcatchem*, **6**, 1774 (2014).
20. M. V. Landau, L. Titelman, L. Vradman and P. Wilson, *Chem. Commun.*, **5**, 594 (2003).
21. X. Wang, *J. Catal.*, **222**, 565 (2004).
22. P. Li, X. Chen, Y. Li and J. W. Schwank, *Catal. Today*, **364**, 7 (2021).
23. P. Li, X. Chen, L. Ma, A. Bhat, Y. Li and J. W. Schwank, *Catal. Sci. Technol.*, **9**, 1165 (2019).
24. J. A. Lupescu, J. W. Schwank, K. A. Dahlberg, C. Y. Seo, G. B. Fisher, S. L. Peczonczyk, K. Rhodes, M. J. Jagner and L. P. Haack, *Appl. Catal. B-Environ.*, **183**, 343 (2016).
25. L. Ma, C. Y. Seo, X. Chen, K. Sun and J. W. Schwank, *Appl. Catal. B-Environ.*, **222**, 44 (2018).
26. J. Luo, M. Meng, Y. Zha and L. Guo, *J. Phys. Chem. C*, **112**, 15293 (2008).
27. L. Ma, C. Y. Seo, X. Chen, K. Sun and J. W. Schwank, *Appl. Catal. B-Environ.*, **222**, 44 (2018).
28. P. Li, X. Chen, Y. Li and J. W. Schwank, *Catal. Today*, **327**, 90 (2018).
29. P. Li, R. Dong, X. Jiang, S. Zhang, T. Liu, R. Wang, F. Yan and D. Fu, *J. Electroanal. Chem.*, **873**, 114513 (2020).
30. L. Ma, C. Y. Seo, X. Chen, J. Li and J. W. Schwank, *Chem. Eng. J.*, **350**, 419 (2018).
31. M. Aghabararnejad, G. S. Patience and J. Chaouki, *Can. J. Chem. Eng.*, **92**, 1903 (2014).
32. S. Hosokawa, R. Tada, T. Shibano, S. Matsumoto, K. Teramura and T. Tanaka, *Catal. Sci. Technol.*, **6**, 7868 (2016).

Supporting Information

CO and C_3H_6 oxidation over $La_{0.9}Sr_{0.1}CoO_3$ catalysts: Influence of preparation solvent

Fei Yan*,, Ping Li*,**,†, and Xia Zhang*****

*Hebei Key Lab of Power Plant Flue Gas Multi-Pollutants Control, Department of Environmental Science and Engineering, North China Electric Power University, Baoding, 071003, P. R. China
**MOE Key Laboratory of Resources and Environmental Systems Optimization, North China Electric Power University, Beijing, 102206, P. R. China
***Advanced Research Institute for Multidisciplinary Science, QiLu University of Technology (Shandong Academy of Science), Jinan 250353, Shandong Province, P. R. China
(*Received 2 December 2020 • Revised 9 March 2021 • Accepted 10 March 2021*)

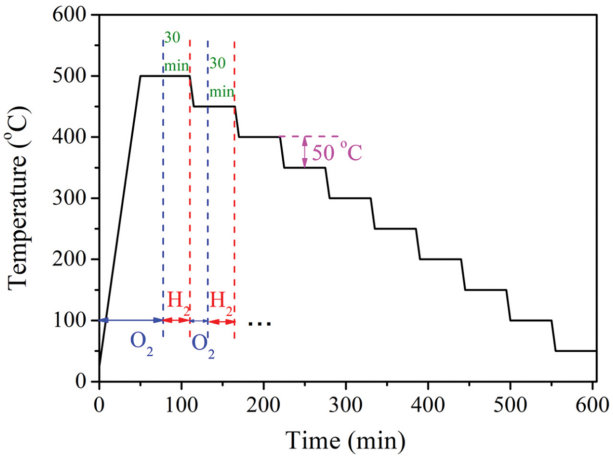

Fig. S1. Oxygen release rate measurements procedure.

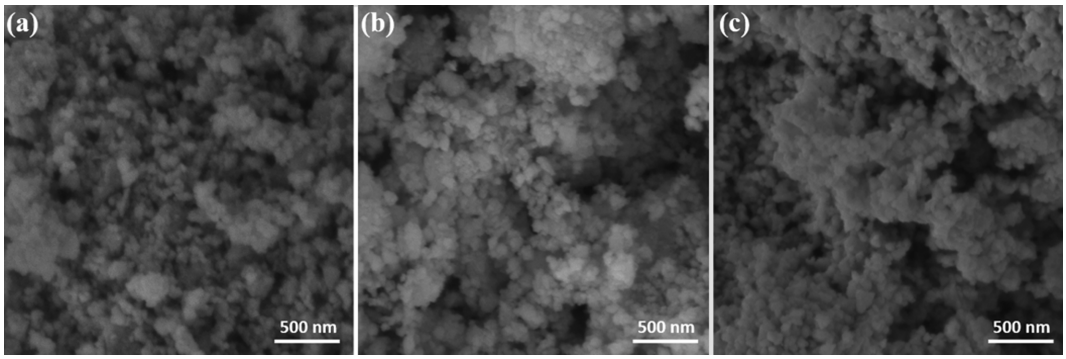

Fig. S2. SEM images of (a) LSCO (E), (b) LSCO (E/W) and (c) LSCO (W).

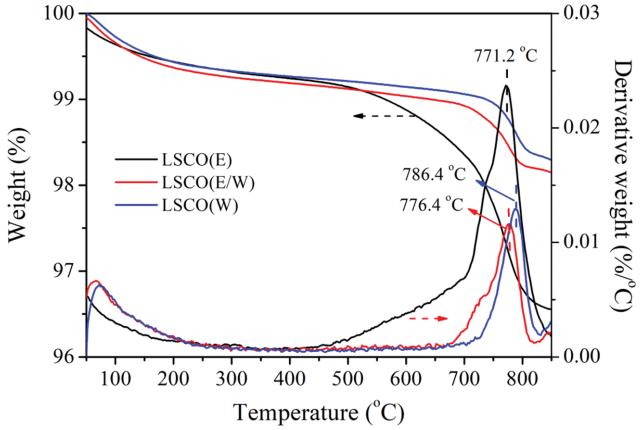

Fig. S3. Thermogravimetric curves of various LSCO catalysts in the N_2 flow.

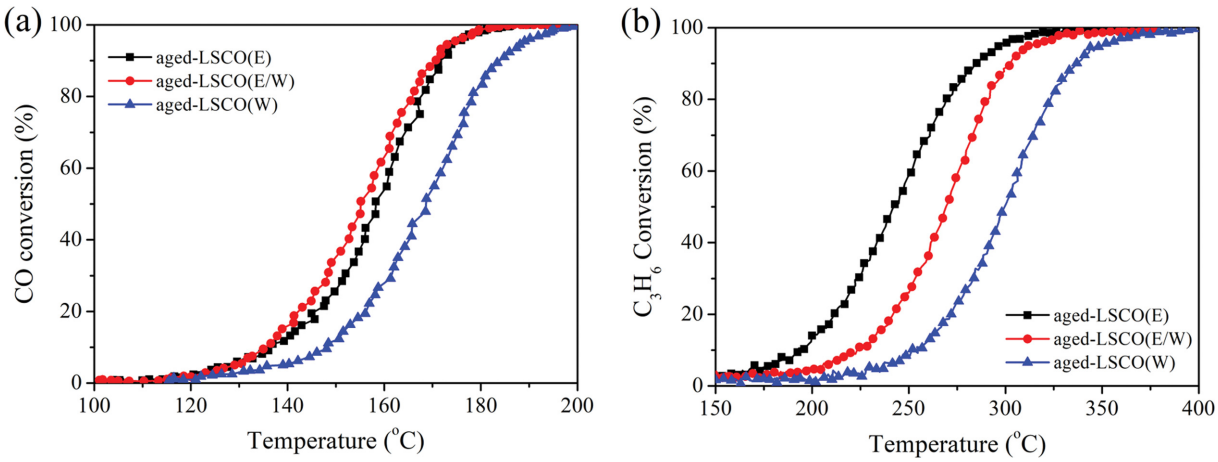

Fig. S4. Light-off curves of (a) CO oxidation and (b) C_3H_6 oxidation over various aged-LSCO catalysts after hydrothermally treated. Reaction conditions: (a) 0.4% CO, 10% O_2 balanced with N_2 and (b) 0.1% C_3H_6, 10% O_2 balanced with N_2.

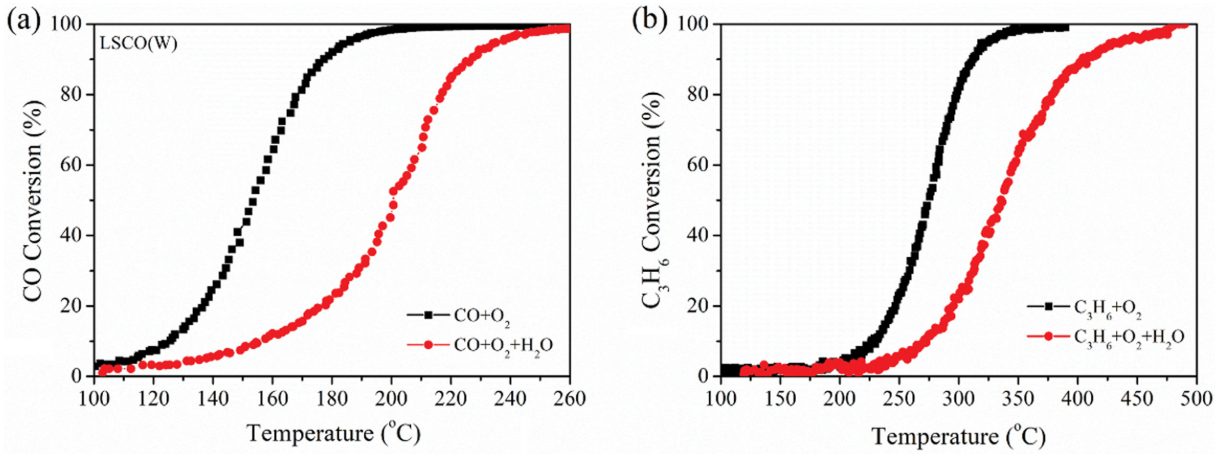

Fig. S5. Light-off curves of (a) CO oxidation and (b) C_3H_6 oxidation over LSCO (W) catalyst at different conditions (■ 0.4% CO, 10% O_2, 5% H_2O balanced with N_2; ● 0.1% C_3H_6,10% O_2, 5% H_2O balanced with N_2).

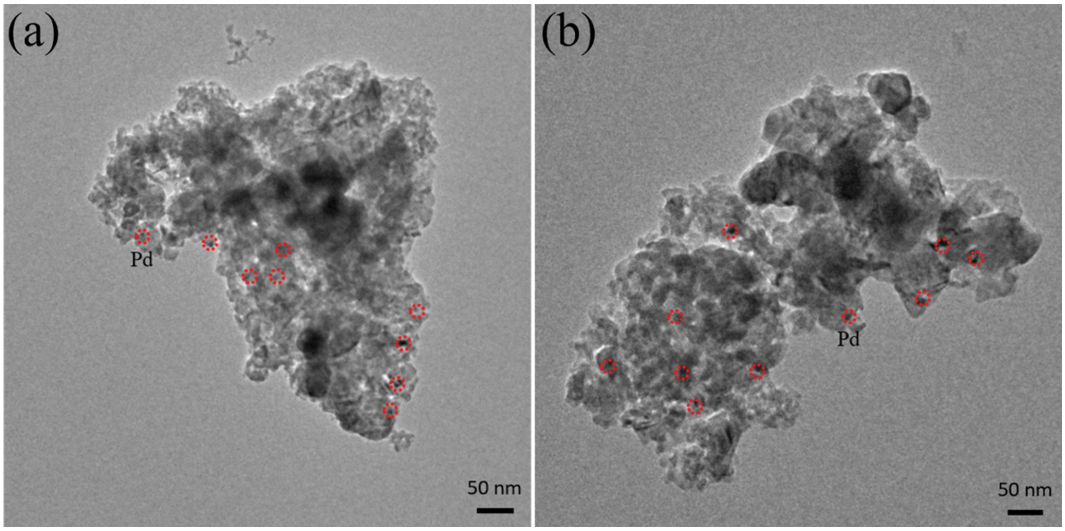

Fig. S6. TEM images of (a) Pd/LSCO (E) and (b) Pd/LSCO (S).

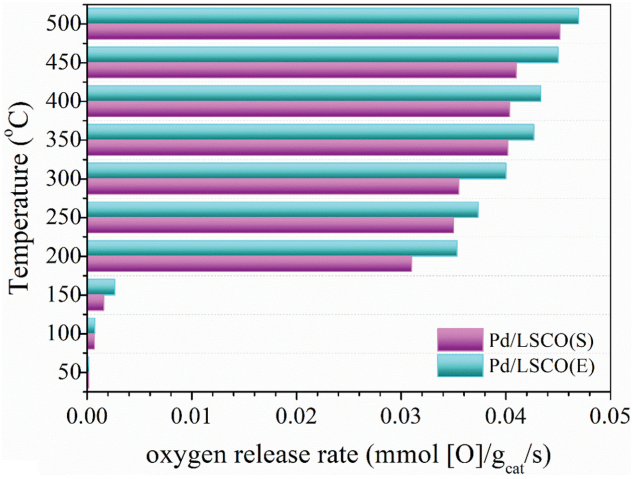

Fig. S7. Oxygen loss rate of Pd/LSCO (E) and Pd/LSCO (S) catalysts under various temperatures.